Environ Geochem Health (2021) 43:2945–2963
https://doi.org/10.1007/s10653-020-00757-2

ORIGINAL PAPER

Characteristics, emission sources and health risk assessment of trace elements in size-segregated aerosols during haze and non-haze periods at Ningbo, China

Liangping Long · Jun He · Xiaogang Yang

Received: 19 November 2019 / Accepted: 13 October 2020 / Published online: 18 January 2021

Abstract To characterize trace elements from inhalable particles and to estimate human health risks, airborne particles at an urban area of Ningbo city during haze and non-haze periods from November 2013 to May 2014 were collected by a nine-stage sampler. Seventeen trace elements (Na, Mg, Al, K, Ca, Ti, V, Cr, Mn, Fe, Co, Ni, Cu, Zn, As, Cd and Pb) were measured by inductively coupled plasma mass spectrometry (ICP-MS). The concentrations of trace elements are in the ranges of 0.51 ng m^{-3} (Co) $\sim$ 1.53 μg m^{-3} (K) for fine particles (Dp $<$ 2.1 μm), and 1.07 ng m^{-3} (Co) $\sim$ 4.96 μg m^{-3} (K) for coarse particles (2.1 μm $<$ Dp $<$ 9.0 μm) during the haze days, which are 1.15 –4.30 and 1.23– 7.83-fold as those of non-haze days, respectively. These elements could be divided into crustal elements (Na, Mg, Al, Ca, Ti, Fe and Co), non-crustal elements (Cu, Zn, Cd and Pb) and mixed elements (K, V, Cr, Mn, Ni and As) according to their enrichment factor values (EFs) and size distribution characteristics. Five emission sources of trace elements were identified by positive matrix factorization (PMF) modeling. The main sources of trace elements in fine particles are traffic emission (21.7%), coal combustion (23.6%) and biomass burning (32.1%); however, soil dust (61.5%), traffic emission (21.9%) and industry emissions (11.8%) are the main contributors for coarse particles. With the help of the multiple-path particle dosimetry (MPPD) model, it was found that deposition fractions of seventeen measured elements in the pulmonary region were in the range of 12.4%–15.1% and 6.66% –12.3% for the fine and coarse particles, respectively. The human health risk assessment (HRA) was employed according to the deposition concentration in the pulmonary region. The non-carcinogenic risk (HI) was below the safety limit

Electronic supplementary material The online version of this article (https://doi.org/10.1007/s10653-020-00757-2) contains supplementary material, which is available to authorized users.

L. Long · J. He (✉)
International Doctoral Innovation Centre, University of Nottingham Ningbo China, Ningbo, Zhejiang, PR China
e-mail: jun.he@nottingham.edu.cn

L. Long · J. He
Department of Chemical and Environmental Engineering, University of Nottingham Ningbo China, Ningbo, Zhejiang, PR China

J. He
Key Laboratory of Carbonaceous Wastes Processing and Process Intensification Research of Zhejiang Province, University of Nottingham Ningbo China, Ningbo, PR China

X. Yang
Department of Mechanical, Material and Manufacturing Engineering, University of Nottingham Ningbo China, Ningbo, Zhejiang, PR China

(1.00). Nonetheless, the excess lifetime carcinogenic risk (ELCR) for adults increased by 2.42-fold during the haze days (2.06×10^{-5}) as compared to that of non-haze days (8.50×10^{-6}) in fine particles. Cr (VI) and As together contributed 96.5% and 96.3% of the integrated cancer risks during the haze and non-haze periods, respectively. Moreover, the related ELCR values in coarse particles were 36.7% and 62.8% of those in the fine particles for the non-haze period and haze period, respectively.

Keywords Haze · Trace elements · Size distribution · Source apportionment · Health risk assessment

Introduction

Haze has attracted much attention worldwide, because of its significant visibility reduction due to the light extinction, negative health effects and impact on regional weather and climate (Behera et al. 2015b; Khare and Baruah 2010). The Yangtze River Delta (YRD) region is one of the well-developed regions in Eastern China, which has experienced considerable haze events owing to its fast industrialization for the past few decades (Fu et al. 2008; Li et al. 2015). Among the different chemical compositions of particulate matter, some non-crustal elements, especially heavy metals such as Cr, Ni, Cd and Pb, have been grouped as toxic because of their negative health effects to human beings (Greene and Morris 2006; Kampa and Castanas 2008). Furthermore, most of the transition metals such as Fe play a dominant role in the production of hydroxyl radicals (OH·), which may trigger cancer or DNA damage to humans (Saffari et al. 2014). Therefore, the understanding of characteristics, sources and associated human health risks of trace elements is of great importance to formulate the targeted actions to control haze episodes.

A number of studies about trace elements in aerosols from Asia found the levels of toxic elements are much higher in urban and/or rural areas as compared to the limit of World Health Organization (WHO) and mainly originated from anthropogenic sources (Fang et al. 2010; Khare and Baruah 2010). In 2007 a four-site (Suzhou, Hangzhou, Shanghai and Nanjing) sampling campaign was conducted in YRD, which found that the EFs of As, Cd and Pb on $PM_{2.5}$ in the heaviest pollution episode were increased by 4.45–6.68 times compared to other days (Fu et al. 2008). Huang et al (2009) collected dozens of atmospheric deposition samples covering the center of YRD and the study revealed a distinct accumulation of most analyzed trace metals compared to the reference values. Wang et al (2014) investigated a very strong haze pollution occurring at YRD including cities of Hefei, Nanjing, Wuxi, Huzhou, Lin'an, etc., in January 2013 by measuring the chemical components on $PM_{0.2–2}$, which showed heavy metals, dust and sea salt composed 12.6% of the particulate mass concentration on non-polluted days, yet these components occupied less than 6% of the particulate mass concentration on polluted days having slight variation with size. Furthermore, previous studies reported that the elemental composition of ambient aerosols of different size varied greatly, largely dependent on the type of the local/regional anthropogenic sources (Gao et al. 2016; Pan et al. 2013; Tan et al. 2016). Hence, just to reduce the aerosol mass concentration may not be the best way to control these particulate toxic metals (Khillare and Sarkar 2012). Therefore, source apportionment of trace elements in size resolved aerosol samples seem essential in prioritizing mitigation measures.

It has been reported that the average daily exposure dose of particulate metals human health risk assessment could depend on the total concentration (Wang et al. 2016), deposition fraction (Behera et al. 2015a; Betha et al. 2014) and bio-accessibility (Mukhtar and Limbeck 2013). Researchers either apply a semi-empirical equation (Behera et al. 2015b; Niu et al. 2015) or MPPD model (Betha et al. 2014; Ham et al. 2011) to evaluate the deposition fraction of the particulate trace elements. The former method is very simple to use and hypothesizes that all elements have the same deposition efficiencies, while the MPPD model is closer to the actual situation of the human lung and its limitation lies in that the samples must be collected by size-segregated samplers. Even for the MPPD model, researchers obtained different results for deposition fractions of trace elements in the pulmonary region. Ham et al. (2011) found the deposition fractions of V and Zn were higher in summer than winter, while Betha et al (2014) found most elements had higher deposition fraction in haze days compared to non-haze days. However, the

relationship between the elemental composition and their deposition fractions on fine and coarse particles has not been well investigated at present.

The present study was conducted to investigate multiple trace elements in size-segregated aerosols collected by a nine-stage Anderson sampler in both haze and non-haze periods in an urban site at Ningbo city from November 2013 to May 2014. The source contributions of these elements were identified by the PMF model. The deposition fractions of toxic elements in the human respiratory system such as head and throat (H), tracheobronchial (T) and pulmonary (P) region have been estimated using the MPPD model. Finally, the human health risks for adults from toxic elements were evaluated and compared for both exposure periods.

Experimental

Sampling

Ningbo is located in the north of Zhejiang province and the south of YRD. Ningbo port is in the top five worldwide and the industrial scale is the top one in the province. Our sampling was conducted on the rooftop of the administration building at Ningbo municipal meteorological bureau in Haishu District of Ningbo (29.87° N, 121.53° E), which was situated in a mixed residential and commercial area with high traffic density and around 10 km away from the East China Sea (Fig. S1). Size-segregated aerosol samples were collected from 15 October 2013 to 16 May 2014 by a low-pressure cascade impactor (TFE 20-800, ThermoFisher, USA) working at the flow rate of 28.3 L min^{-1} based on the method described elsewhere (Li et al. 2012; Pan et al. 2013). Briefly, each set of samples was collected for 23.5 h from 9:00 am to 8:30 am the next day. The sampler can take nine samples in a set with nominal cut-off diameters decrease from top to bottom in 9 stages, which rank as follows: stage 1 (> 9.0 μm), stage 2 (5.8–9.0 μm), stage 3 (4.7–5.8 μm), stage 4 (3.3–4.7 μm), stage 5 (2.1–3.3 μm), stage 6 (1.1–2.1 μm), stage 7 (0.65–1.1 μm), stage 8 (0.43–0.65 μm) and stage 9 (< 0.43 μm). The substrates were 81 mm mixed cellulose microfiber filter and each sample was put into a single plastic case and stored at − 20°C until further extraction and analysis. Meanwhile, meteorological parameters including visibility, wind speed, ambient temperature (T) and relative humidity (RH) were obtained from an automated weather station in the same building during the sampling period. The local air quality index (AQI), together with levels of $PM_{2.5}$ and PM_{10}, was acquired from Ningbo Real-time Air Quality Publication System operated by Ningbo Municipal Environmental Monitoring Center.

Air mass backward trajectory

To monitor the migration of air masses, the Hybrid Single-Particle Lagrangian Integrated Trajectory (HYSPLIT, 4.9 model) was applied for air mass backward trajectory analysis according to the setup from previous studies (Stein et al. 2015). All backward trajectories were generated every 2 h for a total of 96 h backward of the sampling at 500 m above the ground level to ensure the starting trajectory was within the atmospheric boundary layer and remaining close to the ground surface. The cluster analysis for all trajectories was calculated by the latest software of TrajStat (1.2.1.0) (Wang et al. 2009), which was applied successfully by Xu et al. (2016) for the same purpose recently.

Extraction and analysis of trace metals

A half filter of each sample was digested by a microwave digester (MARS 5, CEM, USA) with 10 ml mixture of nitric acid (65%), hydrochloric acid (37%) and purified water (18.2 MΩ cm^{-1}) with a volume ratio of 55.5:167.5:777 (Ho et al. 2006; Tan et al. 2014). The digester was programmed for temperature program as below: the first step was to heat up from room temperature to 185°C in 15 min; the second step was to keep at the temperature for another 25 min. After cooling to room temperature, each digest was filtered through 0.45 μm PTFE membrane filters; then 0.555 ml nitric acid (65%) and 0.5 ml internal standards solution (5 ppm of In, Sc, Y and Ge in 1% nitric acid) were added. After that, the mixture was diluted to 50 ml with purified water (18.2 MΩ cm^{-1}). Then these extracts were refrigerated at 4 °C for further analysis. The concentrations of seventeen trace elements were measured by ICP-MS (Perkin-Elmer 300X, USA). For quality control, elemental concentrations in field blanks were

subtracted from sample concentrations. Also, the corresponding relative standard deviation (RSD) of triplicated measured concentrations in each sample was less than 10% for all elements except Cd with RSD of less than 20%.

Enrichment factors

Enrichment factors (EFs) were used to classify crustal and non-crustal elements (Zoller et al. 1974). The EF of element X in aerosols is defined as below:

$$EF_X = \frac{\left[C_X/C_{Al}\right]_{Air}}{\left[C_X/C_{Al}\right]_{Crust}} \quad (1)$$

where $(C_x/C_{Al})_{Air}$ is a ratio for the concentration of element X to that of Al in particles; $(C_x/C_{Al})_{Crust}$ is the corresponding concentration ratio of element X to Al in the crust. The elemental abundance of the crust was referenced from Taylor and McLennan (1995). If EF_X is close to unity, crustal soil is the overwhelming majority source for element X (Zoller et al. 1974). And if EF_X is over 10, the element X would have prominent sources from anthropogenic emissions (Behera et al. 2015a). The element X has mixed sources if EF is in the range of 1 to 10.

Source apportionment

PMF receptor model (version PMF 5.0) was used in this study to quantify emission sources of trace elements. Concentrations of 18 species (17 measured elements including Na, Mg, Al, K, Ca, Ti, V, Cr, Mn, Fe, Co, Ni, Cu, Zn, As, Cd and Pb, and the sum of these elements) of 108 samples (9 samples per sets × 12 sets) were formed as the input dataset. Uncertainties (Unc) of these species were calculated according to Eq. (2) and (3) (Huang et al. 2018). Equation (2) was used when concentrations of species were ≤ the method detection limit (MDL), and Eq. (3) was applied when concentrations were above related MDLs:

$$Unc = \frac{5}{6} \times MDL \quad (2)$$

$$Unc = \sqrt{(\boldsymbol{ErrorFraction} \times \boldsymbol{concentration})^2 + (0.5 * MDL)^2} \quad (3)$$

An Error Fraction was set as 10% for both haze and non-haze samples. Only converged solutions should be investigated for further analysis. Na, V, Ni, As and the sum were grouped as weak species due to low correlation coefficients between observed and predicted values.

Elements deposition modeling

Various studies have assessed the deposition of particulate matter from the ambient air in H, T and P region of the respiratory system of human beings by using the deposition models (Betha et al. 2014; Youn et al. 2016). The most widely used regional lung deposition models are the International Commission on Radiological Protection (ICRP) deposition model and the MPPD model. The former is a simple path model that is not suitable for calculating the particle deposition for a defined region (Hofmann 2011). Therefore, the MPPD model had been employed to calculate the deposition fraction efficiencies for elements in size-segregated samples successfully in previous studies (Betha et al. 2014; Lyu et al. 2017; Wang et al. 2019), which would be applied in this study too.

Input data including airway parameters, particle properties and exposure conditions are needed to run the MPPD model. In this modeling, the adjustable assumptions include the following points: Yeh-Schum Single path; the object is a human adult with functional reserve capacity, upper respiratory tract and the tidal volume are 3300 ml, 50 ml and 625 ml, respectively; nasal breathing of spherical particles at a frequency of 12 breaths min^{-1}; the inspiratory fraction is 0.5. The multiple diameters (0.1–10 μm) is selected because it is very close to the real formation of the human airway (Betha et al. 2014; Lyu et al. 2017). Fine particle mass density was hypothesized as 1.66 g cm^{-3} and 1.78 g cm^{-3} based on the polluted days and clean days in Beijing, respectively (Li et al. 2016). The deposition concentration (DC, ng m^{-3}) of individual metal is estimated by

$$DC = \sum (C_i \times DF_i) \quad (4)$$

where DF_i is the deposition fraction of trace elements in three regions (H, TB and P) of the human respiratory tract; C_i (ng m^{-3}) is the concentration of individual trace elements in each size bin.

Health risk assessment

In this study, the health risk assessment model of USEPA has been applied for the human health risk evaluation (USEPA, 2009). V, Cr(VI), Mn, Co, Ni, As and Cd are grouped as toxic elements that have non-carcinogenic health risks in the human body, while Cr(VI), Co, Ni, As, Cd and Pb are classified as carcinogens to human health (USEPA, 2015). HRA was performed based on elemental concentrations in fine and coarse particles for hazard quotient (HQ) and excess lifetime cancer risk (ELCR) (USEPA 2009). Cr(VI) concentration was assumed 1/7 of Cr concentration (Taner et al. 2013). Only adults and the inhalation pathway (EC_{inhale}) are considered for the exposure mode in the present study (Betha et al. 2014; Huang et al. 2018). The equations for the calculation of HRA are as follows:

$$EC_{inhale} = \frac{C_{UCL} \times ET \times EF \times ED}{AT_n}$$

$$HQ_{inh} = \frac{EC}{RfC_i \times 1000 \mu g/mg}$$

$$HI = \sum HQ_i$$

$$CR_{inh} = IUR \times EC$$

where C_{UCL} is the upper limit of the 95% confidence interval for the mean (μg m^{-3}) (Zhang et al. 2018); *ET* is the exposure time (24 $hday^{-1}$); *EF* is exposure frequency (350 $daysyear^{-1}$ for residents); *ED* is exposure duration (24 years for adults and 6 years for children); AT_n is the average time (for non-carcinogens, $AT_n = ED \times 365$ days $\times$ 24 $hday^{-1}$; for carcinogens, $AT_n = 70$ years $\times$ 365 $daysyear^{-1}$ $\times$ 24 h). RfC_i and *IUR* stand for inhalation reference concentrations (mgm^{-3}) and inhalation unit risk ($m^3\mu g^{-1}$), respectively (USEPA 2015). Hazard index (*HI*) is the sum of *HQ* for different elements (USEPA 2009). The safety limits of *HQ* and *HI* are 1.00, exceeding the limit suggests non-carcinogenic risk. If *ELCR* is less than 10^{-6}, the cancer risk can be ignored.

Results and discussion

Categorization of haze and non-haze periods

To investigate and compare the variations of trace elemental profiles in aerosols of Ningbo under different polluted conditions, the samples were divided into the haze and non-haze periods. Sampling days with visibility below 10 km, RH less than 90% and $PM_{2.5}$ mass concentration above 75 μgm^{-3} were classified as haze periods, while the sampling days with visibility above 10 km, RH below 90% and $PM_{2.5}$ mass concentration below 75 μgm^{-3} were classified as non-haze periods (Mishra et al. 2015; Xu et al. 2015). Based on the classification of haze and non-haze periods, 12 sets of samples were chosen for this study, of which 5 sets were from the non-haze periods, and 7 sets were from the haze periods. Table 1 shows the AQI, occurrence levels of $PM_{2.5}$ and PM_{10}, T, RH, wind speed and visibility of both periods. High AQI values (147 ± 25.7), dry weather condition (RH: 55.4% ± 12.3%), with poor visibility (4.60 ± 1.70 km) and weak surface wind (1.60 ± 0.800 m s^{-1}) were observed during the haze days. However, low AQI values (58.2 ± 18.1), moist weather condition (RH: 70.6% ± 14.7%) with high visibility (14.9 ± 4.30 km) and higher surface wind speed (2.5 ± 0.5 m s^{-1}) were observed in the non-haze days. The mass concentrations of $PM_{2.5}$ and PM_{10} in the haze periods (117 ± 17.0 μg m^{-3} and 182 ± 26.0 μgm^{-3}) were about 4 times of those in the non-haze periods (30.0 ± 12.0 μg m^{-3} and 47.0 ± 14.0 μg m^{-3}). Besides, the mass concentrations of $PM_{2.5}$ and PM_{10} during haze days were much higher than the WHO 24-h average standards with 25 μg m^{-3} and 50 μg m^{-3} for $PM_{2.5}$ and PM_{10}, respectively; and they also violated the level 2 daily average thresholds of 75 μg m^{-3} and 150 μg m^{-3} by the Chinese National Ambient Air Quality Standards (GB 3095-2012). This suggests that the local public may suffer negative health effects to a certain degree due to the exposure of these high levels of particulate matter during the haze days.

Air mass backward trajectory

Figure 1 shows 96 h of air mass backward trajectories at 500 m (above ground level) with 2-h intervals for both study periods. As for the haze period, the wind generally brought the air masses from Northwest China. Two clusters together with 60.7% of the air mass passed from Xinjiang, Gansu, Inner Mongolia, Ningxia, north of Shaanxi, south of Shanxi, Henan and Anhui provinces to Ningbo. Another cluster with the other 39.3% of air mass came from south of Shanxi,

Table 1 Aerosol concentrations and meteorological conditions

Sampling date (dd/mm/yyyy)		AQI	$PM_{2.5}$ (μgm^{-3})	PM_{10} (μgm^{-3})	Temp (°C)	RH (%)	WS ($m\ s^{-1}$)	Vis (km)
Haze days	15/11/2013	118	113	175	13	72	2.5	2.6
	29/12/2013	123	112	173	1	44	1.4	6.4
	30/12/2013	152	113	175	4	45	1.1	5.9
	31/12/2013	136	98	154	6	48	0.8	6.4
	03/01/2014	180	139	213	11	59	1.7	4.1
	04/01/2014	182	141	225	8	48	2.8	4.1
	05/01/2014	138	103	162	6	72	1.1	2.8
	Average	147 ± 26	117 ± 17	182 ± 26	7 ± 4.1	55 ± 12	1.6 ± 0.8	4.6 ± 1.6
Non-haze days	05/05/2014	60	25	53	16	56	2.8	20.5
	10/05/2014	47	21	34	20	88	2.8	14.2
	11/05/2014	37	18	30	22	84	2.8	17.7
	12/05/2014	85	46	62	22	67	1.7	9.6
	13/05/2014	62	39	57	20	58	2.5	12.4
	Average	58 ± 18	30 ± 12	47 ± 14	20 ± 2.4	71 ± 15	2.5 ± 0.5	15 ± 4.3

north of Henan, and pass over Jiangsu from north to south direction (Fig. 1a).This cluster travelled a much shorter distance, indicating a more stagnant meteorological condition near the receptor site. Hence, this site was significantly affected by industrial emissions. Regarding the non-haze days, the wind direction was quite different. Of which 18.3% of the air masses came from the northwest, 20% of the air mass passed over from Siberia, East of Mongolia, Beijing, Hebei, Shandong and over the Yellow Sea before reaching Ningbo. The remaining 61.7% of the air masses reaching Ningbo originated from the East China Sea and travelled a much shorter distance (Fig. 1b). These ocean region air masses brought aerosols mainly emitted from ships and local sources of the coast region. Therefore, it appears that the particulate matter was characteristic with crustal and industrial emission aerosols during the haze days, but typically with sea salt, ship emission aerosols during the non-haze days.

Elemental characterization

Elemental concentrations

In the present study, fine ($Dp < 2.1\ \mu m$), coarse ($2.1\ \mu m < Dp < 9.0\ \mu m$) and large ($Dp > 9.0\ \mu m$) particles were defined due to no cut-off sizes of 2.5 and 10 μm in the sampler. Table 2 lists the average concentrations of seventeen trace elements among fine, coarse and large particles at Ningbo during the haze and clear periods. The elemental concentrations of each stage are also presented in Fig. 2.

The results in Table 2 show that the elemental concentrations of the selected seventeen trace elements (TEs) in fine particles during the haze period ranged from 0.510 ng m^{-3} (Co) to 1.53 μg m^{-3} (K) with a sum of 5.53 μg m^{-3}, which is about a third as that of coarse particles but 3 times that of large particles. However, the occurrence levels of TEs in fine particles were quite different during the non-haze days, with a range of 0.240 ng m^{-3} (Co) to 1.52 μg m^{-3} (Ca). The sum of seventeen TEs in fine and coarse particles was 3.49 and 5.60 μg m^{-3}, respectively; however it was only 0.750 μg m^{-3} in the large particles. Moreover, all elements except Ca in fine particles showed higher concentration during the haze periods. The ratios of elemental concentrations between haze and non-haze periods were in the range from 1.15 (Na) to 4.30 (Zn) for fine particles and 1.23 (Na) to 7.82 (Cd) for coarse particles. This suggests that the elemental pollution in the haze period was much stronger compared to the non-haze period.

As shown in Table 2, the concentration of Cr (VI) was 25 ∼ 202 times higher than the limit for Cr(VI) (0.025 ng m^{-3}) from National Ambient Air Quality Standards (NAAQS) in China (MEP 2012). The

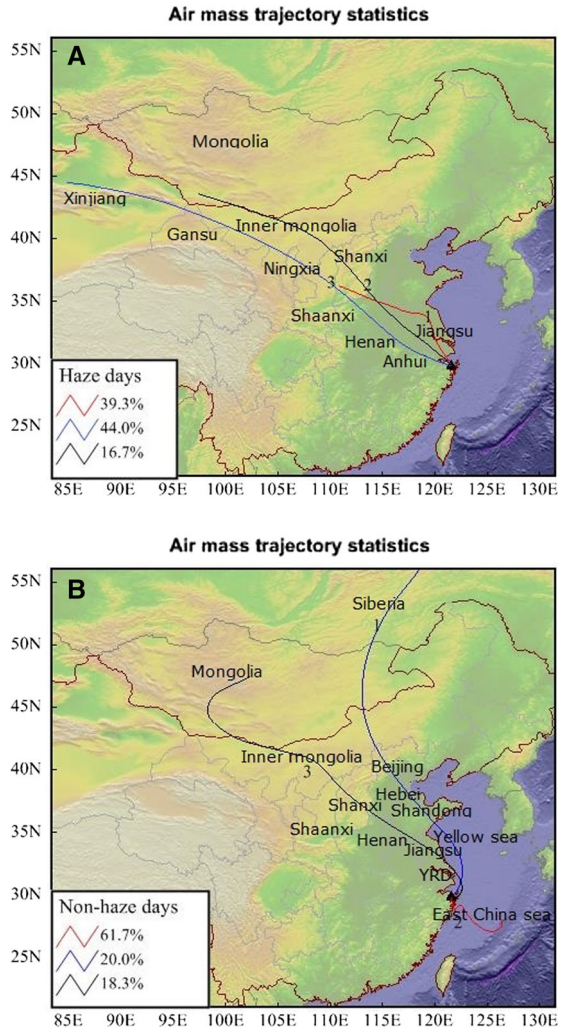

Fig. 1 The 96 h air mass backward trajectories of Ningbo with an interval of 2 h at 500 m (above ground level) during the haze **(a)** and non-haze **(b)** days

concentrations of As in fine and coarse particles were about three times higher than the concentration limit for As (6 ng m^{-3}) from NAAQS in China (MEP 2012). However, the levels of Cd and Pb were lower than guideline values of NAAQS in China (5 ng m^{-3} for Cd; 500 ng m^{-3} for Pb) (MEP 2012). The concentrations of Mn and Ni were within the target values of WHO (150 ng m^{-3} and 25 ng m^{-3} for Mn, Ni, respectively) (WHO 2000). To compare with studies from other parts of China, the mean concentrations of some elements in the fine particles during the haze days are presented (Table 3). It was observed that most of the elements are comparable with other cities such as Shanghai (Behera et al. 2015b), Guangzhou (Cao et al. 2012) and Beijing (Yang et al. 2010). This finding suggests Ningbo also suffers from atmospheric element pollution like other cities in China.

Figure S2 presents the percentage of elemental concentration in the fine, coarse particles and large particles to the sum of 9 stages for both periods. Na, Mg, Al, Ca, Ti, Fe and Co are mainly in coarse particles. K, Mn, Cu, Zn, Cd and Pb are mainly distributed in fine particles. It should be noted that V, Cr, Ni and As are distributed in both fine and coarse particles. The elemental fractions of large particles to total suspended particles (TSP) for all elements were in the range of 1.38% ± 0.300% (Cd) to 24.9% ± 2.55% (Cd) in the haze period and from 1.21% ± 0.120% (Cd) to 17.9% ± 4.36% (Cr) in the non-haze period. As most of these TEs that dominated in fine and coarse particles are toxic heavy metals, it can be summarized that TEs were concentrated in both fine and coarse particles.

The major elements were Na, Mg, Al, K, Ca, Fe and Zn, with concentrations higher than 200 ng m^{-3} during the haze period, which constituted 93.2 ± 0.800% and 95.0 ± 1.30% of all elements in fine particles for haze and non-haze periods, respectively. Regarding the coarse particles, these major elements made up of 96.0 ± 0.700% and 96.6 ± 0.700% for the haze and clear days. The sum of the other ten elements only contributed about 5% of the total elemental mass, but most of them are toxic heavy metals such as Cr, Ni, As, Cd and Pb. Therefore, these trace elements could bring huge health risks to humans, especially carcinogenic risks.

The total mass concentrations of the seventeen elements contributed 4.8 ± 0.7% and 13.1 ± 6.20% for $PM_{2.1}$, and 9.30 ± 1.70% and 17.1 ± 5.40% for $PM_{9.0}$ during the haze and non-haze periods, respectively. Li et al. (2012) reported that the total mass concentration of 21 studied elements accounted for 12.5% of the total aerosol mass. Besides, according to the method of Yan et al. (2012), our results show that soil crust was 7.20 ± 1.10% and 27.2 ± 11.6% for $PM_{2.1}$, and 26.7 ± 5.50% and 45.1 ± 12.5% for $PM_{9.0}$ for haze and non-haze periods, respectively. The lower contribution of soil dust in the haze period for $PM_{9.0}$ and $PM_{2.1}$ may indicate that more organic matter was emitted and more secondary aerosols formed during the haze periods, because previous

Table 2 Concentrations of trace elements in size-resolved particles at Ningbo in haze and clear periods

	Haze			Clear/Non-haze		
	Fine (< 2.1 μm)	Coarse (2.1–9.0 μm)	Large (> 9.0 μm)	Fine (< 2.1 μm)	Coarse (2.1–9.0 μm)	Large (> 9.0 μm)
Na (μg m^{-3})	0.63 ± 0.22	0.94 ± 0.53	0.32 ± 0.14	0.55 ± 0.18	0.76 ± 0.20	0.27 ± 0.11
Mg (μg m^{-3})	0.22 ± 0.05	0.80 ± 0.23	0.32 ± 0.11	0.13 ± 0.02	0.34 ± 0.18	0.09 ± 0.04
Al (μg m^{-3})	0.39 ± 0.05	2.27 ± 0.38	0.69 ± 0.16	0.31 ± 0.03	0.77 ± 0.27	0.17 ± 0.06
K (μg m^{-3})	1.53 ± 0.36	1.09 ± 0.24	0.31 ± 0.05	0.41 ± 0.18	0.42 ± 0.19	0.14 ± 0.10
Ca (μg m^{-3})	1.03 ± 0.23	4.96 ± 1.21	2.02 ± 0.66	1.52 ± 0.51	2.07 ± 0.93	0.48 ± 0.23
Ti (ng m^{-3})	41.15 ± 5.48	126.09 ± 17.07	39.88 ± 8.81	23.11 ± 5.89	35.26 ± 17.77	11.35 ± 6.64
V (ng m^{-3})	13.53 ± 3.72	13.14 ± 3.59	3.16 ± 1.05	6.52 ± 0.80	6.47 ± 1.64	1.68 ± 0.30
Cr (ng m^{-3})	32.52 ± 8.08	35.47 ± 9.03	12.06 ± 2.48	12.46 ± 2.98	8.09 ± 1.50	4.40 ± 0.63
Mn (ng m^{-3})	58.18 ± 13.38	50.88 ± 8.92	17.33 ± 4.17	26.01 ± 15.33	17.41 ± 8.05	4.26 ± 2.07
Fe (μg m^{-3})	0.54 ± 0.12	1.55 ± 0.20	0.50 ± 0.13	0.23 ± 0.07	0.49 ± 0.24	0.11 ± 0.06
Co (ng m^{-3})	0.51 ± 0.12	1.07 ± 0.19	0.36 ± 0.11	0.24 ± 0.07	0.45 ± 0.17	0.08 ± 0.03
Ni (ng m^{-3})	9.24 ± 3.36	9.45 ± 3.09	2.76 ± 0.97	5.70 ± 0.89	3.90 ± 0.76	0.36 ± 0.17
Cu (ng m^{-3})	45.53 ± 17.75	23.43 ± 9.07	5.59 ± 1.96	28.22 ± 9.85	12.90 ± 2.70	1.00 ± 0.44
Zn (ng m^{-3})	827.89 ± 79.30	365.99 ± 87.49	54.26 ± 27.76	192.71 ± 40.36	78.54 ± 22.65	8.02 ± 2.54
As (ng m^{-3})	14.37 ± 1.47	13.80 ± 2.15	4.21 ± 0.78	9.81 ± 1.02	9.26 ± 2.03	2.60 ± 0.39
Cd (ng m^{-3})	4.80 ± 1.58	1.09 ± 0.43	0.08 ± 0.02	1.53 ± 0.06	0.14 ± 0.06	0.02 ± 0.01
Pb (ng m^{-3})	154.60 ± 30.16	25.93 ± 4.26	4.67 ± 1.13	54.78 ± 8.14	9.38 ± 1.56	2.08 ± 0.74
$\sum$ (μg m^{-3})	5.53 ± 0.84	15.00 ± 3.04	1.59 ± 0.51	3.49 ± 0.84	5.60 ± 2.00	0.75 ± 0.27

studies found that secondary organic and inorganic aerosols increased during the haze periods (Huang et al. 2014; Sun et al. 2006).

Fig. S3 depicts the EFs of trace elements in the fine, coarse and large particles of both periods. The EFs of Na, Mg, Al, Ca, Mn, Fe and Co are around 1–10, indicating their crustal origin. The EFs of Cr, Cu, Zn, Cd and Pb are within 10–1000, suggesting their non-crustal origin. The EFs of K, Mn and Ni are less than 10 in coarse and large particles but higher than 10 in the fine particles, which signifies that their crustal origin in coarse and large size and non-crustal origin in fine size. Furthermore, the EFs of crustal elements are very similar in both coarse and large particles (e.g. Al, Ca and Fe), while those of non-crustal elements decreased from fine to coarse particles, suggesting that these non-crustal elements were more concentrated in the fine particles. Like the concentrations of trace elements, the EFs of most elements (K, Cr, Mn, Fe, Co, Ni, Cu, Zn, Cd and Pb) were higher in the haze period. The relatively higher EF values of most elements during the haze period could be ascribed to the effects of a massive amount of non-crustal sources such as anthropogenic emissions.

Size distribution

The size distribution of trace elements for both periods is presented in Fig. 3. All seventeen elements are classified as three groups based on concentration patterns as a function of particle size. The first group includes Na, Mg, Al, Ca, Ti, Fe and Co. These metals showed a unimodal distribution in the coarse mode with a single peak in the range from 5.8 to 9.0 μm, which implies that they mainly came from soil and mineral dust (Li et al. 2012), and also possessed the higher elemental concentrations in the larger size bins (Fig. 3).

The second group contains elements such as Zn, Cd and Pb. These elements also have a unimodal

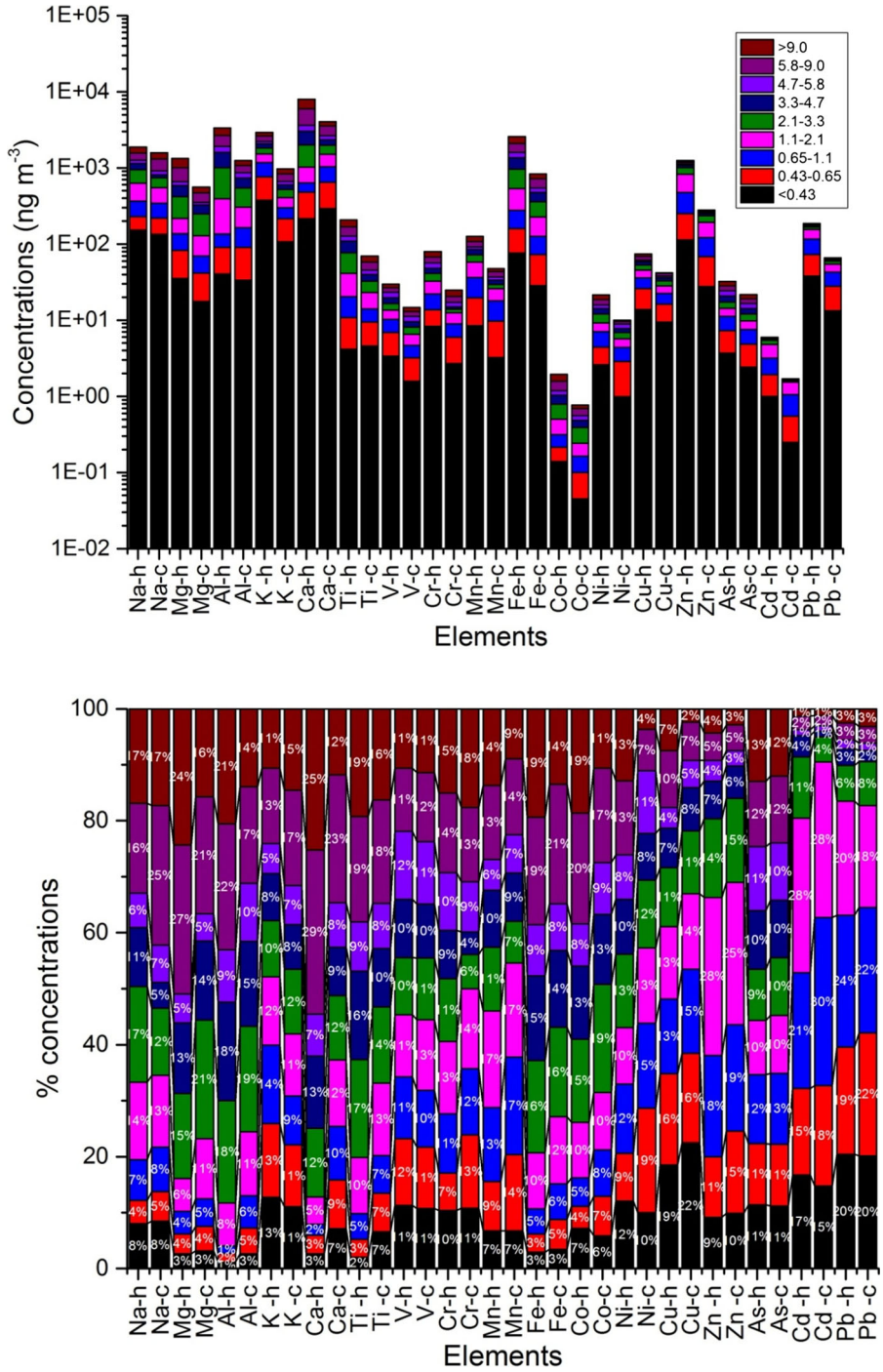

Fig. 2 Absolute and relative concentrations of elements in 9 size bins (the element X–h: haze samples; the element X-c: non-haze samples)

distribution, but mainly peaked in the fine mode within the range of 0.67–1.1 μm, indicating most of them are from anthropogenic sources, while other elements including K, V, Cr, Mn, Ni, Cu and As belong to the third group with a bimodal distribution for one peak at 0.65–1.1 μm and another peak at 4.7–5.8 μm,

respectively. The distribution pattern indicates that elements in the third group are from both natural and anthropogenic emissions-re-suspended dust containing toxic elements. While K, Mn and Ni have EFs less and above 10 values, other metals like Cr and Cu are with EFs above 10 indicating their man-made sources. Their second peak in the coarse mode signifies their re-suspending after being deposited on the grounds. However, the size distribution is very similar in both periods for most of the elements except Co and Zn, both elements shift from unimodal distribution in haze days to bimodal distribution in non-haze days. This might indicate their sources are different in both episodes.

It is reported that mass median aerodynamic diameter (MMAD) of particle mass can display a larger particle size in the haze period (Behera et al. 2015a, b). It might start with a gas-to-particle conversion to form new particles on haze days when RH is higher than 70% (Tao et al. 2014). Although we did not get the size distribution of particle mass as weighing analysis was not employed in the present study, the MMAD of elements in both periods was estimated by the method of O'Shaughnessy and Raabe (2003). For $PM_{2.1}$, MMAD of elements ranges from 0.35 (K) to 0.79 μm (Al), and 0.44 (Zn) to 2.03 (Al) μm for non-haze and haze periods, respectively. For $PM_{9.0}$, the related MMAD of elements are between 0.33 μm and 3.11 μm, and between 0.49 μm to 3.92 μm for the non-haze and haze periods. It indicates that MMADs of elements are larger in the haze period. Since the MMAD was one of the parameters for calculating deposition fractions of particles via the MPPD model (Behera et al. 2015a; Lyu et al. 2017), the change of MMADs may affect deposition fractions of elements in the human respiratory system.

Fig. 3 Size distribution of the trace elements on haze days (the light blue line) and non-haze days (the dark blue line) in Ningbo

Source apportionment by PMF

PMF can quantify the contribution of each source. Eighteen species of 108 samples are formed as the input dataset. Five factors including traffic emissions, coal combustion, soil dust, biomass burning and industry emissions were identified. The source profiles and normalized concentration of each source are displayed in Fig. S4 and S5, respectively. Factor 1 was identified as traffic emissions, as the concentration of

Table 3 Elemental concentrations in the fine particles during the haze days from the present and other studies in China

Study site	Ningbo	Shanghai	Beijing	Guangzhou
Particle type	$PM_{2.1}$-haze	$PM_{1.8}$-haze	$PM_{2.1}$-haze	$PM_{2.5}$-winter
Na (μg m^{-3})	0.63		0.81	
Mg (μg m^{-3})	0.22		0.23	
Al (μg m^{-3})	0.40	0.34	0.50	
K (μg m^{-3})	1.53		1.67	
Ca (μg m^{-3})	1.03		1.52	
Ti (ng m^{-3})	41.15			
V (ng m^{-3})	13.53			
Cr (ng m^{-3})	32.52	18.7		
Mn (ng m^{-3})	58.18	43.4	54.8	60
Fe (μg m^{-3})	0.54	0.53	0.88	0.78
Co (ng m^{-3})	0.51			
Ni (ng m^{-3})	9.24	24	22.9	
Cu (ng m^{-3})	45.53	35.2	66	
Zn (μg m^{-3})	0.83	0.47	0.43	0.59
As (ng m^{-3})	14.37			
Cd (ng m^{-3})	4.80	2.5	3.2	
Pb (ng m^{-3})	154.60	187.7	184.6	420
Reference	This study	Behera et al. 2015a b	Yang et al. 2010	Cao et al. 2012

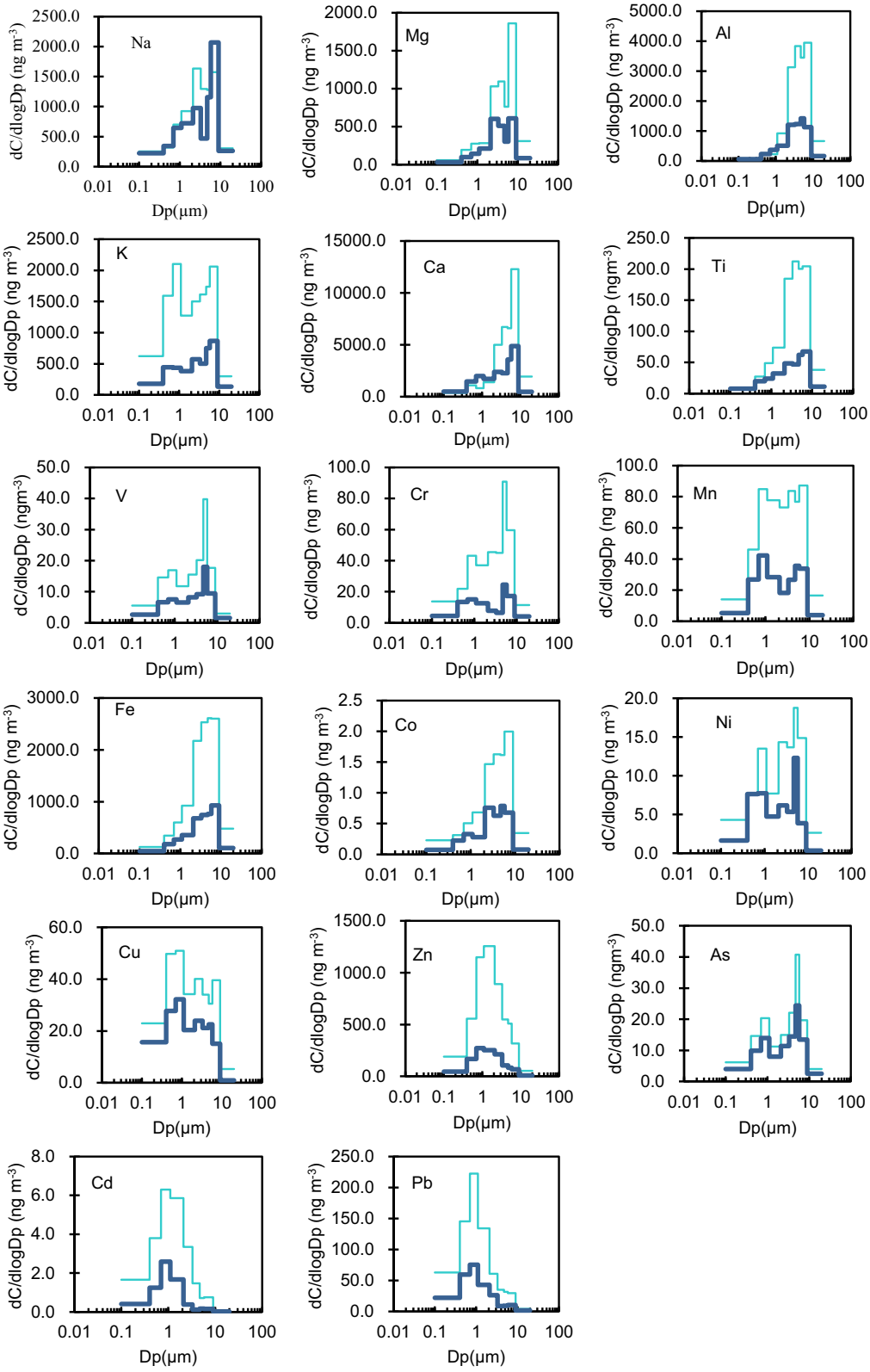
Na
Mg
Al
K
Ca
Ti
V
Cr
Mn
Fe
Co
Ni
Cu
Zn
As
Cd
Pb
dC/dlogDp (ng m-3)
dC/dlogDp (ngm-3)
Dp(μm)
0.01 0.1 1 10 100

this factor to the sum of elements was not changed a lot from haze to non-haze days (Jeong et al. 2019). High contributions were both for large and fine particles (Fig. S5), suggesting both from natural and anthropogenic sources. Factor 2 was coal combustion with high loadings of As and Pb (Tian et al. 2014). High concentrations were mainly for fine particles (Fig. S5). Factor 3 was characterized by high loadings of crustal elements, and high contributions were observed for large and coarse particles, indicating their natural sources. The contribution to the sum of elements was as high as 45.6%. Therefore, this factor was mainly from road dust. Factor 4 was with strong loadings of K, Mn, Zn, Cd and Pb (Fig. S4), and they were concentrated in fine particles, suggesting elements from this factor mainly from anthropogenic sources; besides, we also observed much stronger concentration in haze days than non-haze days. K is often used as a marker element of biomass burning (Andreae et al. 1998). Therefore, this factor was identified as biomass burning. Factor 5 was associated with Cr, Fe and Ni, contributions. It was identified as industrial emissions. Cr is a typical pollutant from power plants and industries (Cheng et al. 2014; Liu et al. 2018). A previous study at Ningbo also found Cr as a single industry emission source (Wang et al. 2018a). This component could be classified as Cr industry emission.

Figures 4 and 5 present absolute and relative concentration of each source to the sum of elements in size bins, fine, coarse and large particles during haze and non-haze days. As shown in Fig. 4, soil dust was mainly distributed in the first 5 stages, coal combustion and biomass burning were kept to the last four stages. Industry emissions were equally distributed in all size bins, but traffic emissions were more concentrated in the first three and last four stages. It is displayed in Fig. 5 that large and coarse particles are mainly formed with a large amount of soil dust (55.5% and 61.5%), traffic emissions (38.3% and 21.9%) and moderate fraction of industry emissions (5.53% and 11.8%), respectively. The sources of fine particles are rich in all sources, especially traffic emissions (21.7%), coal combustion (23.6%) and biomass burning (32.1%). Compared with non-haze days, the source composition of fine particles in haze days was characteristic with stronger emission of coal combustion (1.45 vs. 0.750 μg m^{-3}), biomass burning (2.35 vs. 0.49 μg m^{-3}) and industry emissions (1.02 vs. 0.110 μg m^{-3}), but weaker for soil dust (0.320 vs. 0.700 μg m^{-3}) and traffic emissions (0.730 vs. 1.54 μg m^{-3}). The enhanced source emissions during the haze period provided evidence for the results of air mass backward trajectory in the previous section, which suggested that stronger emissions in the haze period may be a combination of local emissions and regional transboundary transport.

Health risk assessment

Airway fraction deposition

The deposition fraction of particles for both periods along with results of ICRP model is shown in Fig. S6. There are similar distribution of deposition fractions in different regions for both MPPD and ICRP models. However, less total deposition fractions by ICRP model were observed for stage 8 (0.43–0.65) and stage 9 (< 0.43). The difference may be explained that MPPD is a physiologically more realistic model (Kastury et al. 2017; Lyu et al. 2017).

As can be seen from Fig. S6, for large particles in stage 9, the deposition fraction for P is 0.130% in haze days and 0.090% in non-haze days. This is not significant for the health risk assessment of toxic elements in large particles. For fine particles in stage 6–9 and coarse particles in stage 2–5, the deposition fractions in H, T and P region are in the range of 4.89%-91.9%, 3.70%-8.90% and 0.980%-18.3%, respectively. Lower deposition fractions in H for haze days were observed in all stages. Moreover, in the P region, lower deposition fractions were observed in fine particles while those in coarse particles were higher for haze days. As shown in the previous section, the percentage of soil dust in PM_{10} was 28.2% in haze days, which increased to 50.8% in non-haze days. A previous study found that the chemical composition shift affects the material density of PM_{10}; it increased from 1.66 g cm^{-3} in polluted episodes to 1.78 g cm^{-3} in clean episodes (Hu et al. 2012). Therefore, the change of chemical composition between haze and non-haze period is the main driver for having the different deposition fractions in three regions of the respiratory system.

Figure 6 shows deposition fractions of trace elements in the H, T and P region for fine and coarse particles in both periods. For elements in fine particles, it illustrates that the sum of deposition fractions in three regions is approximately 33.9% (Cu) – 49.8%

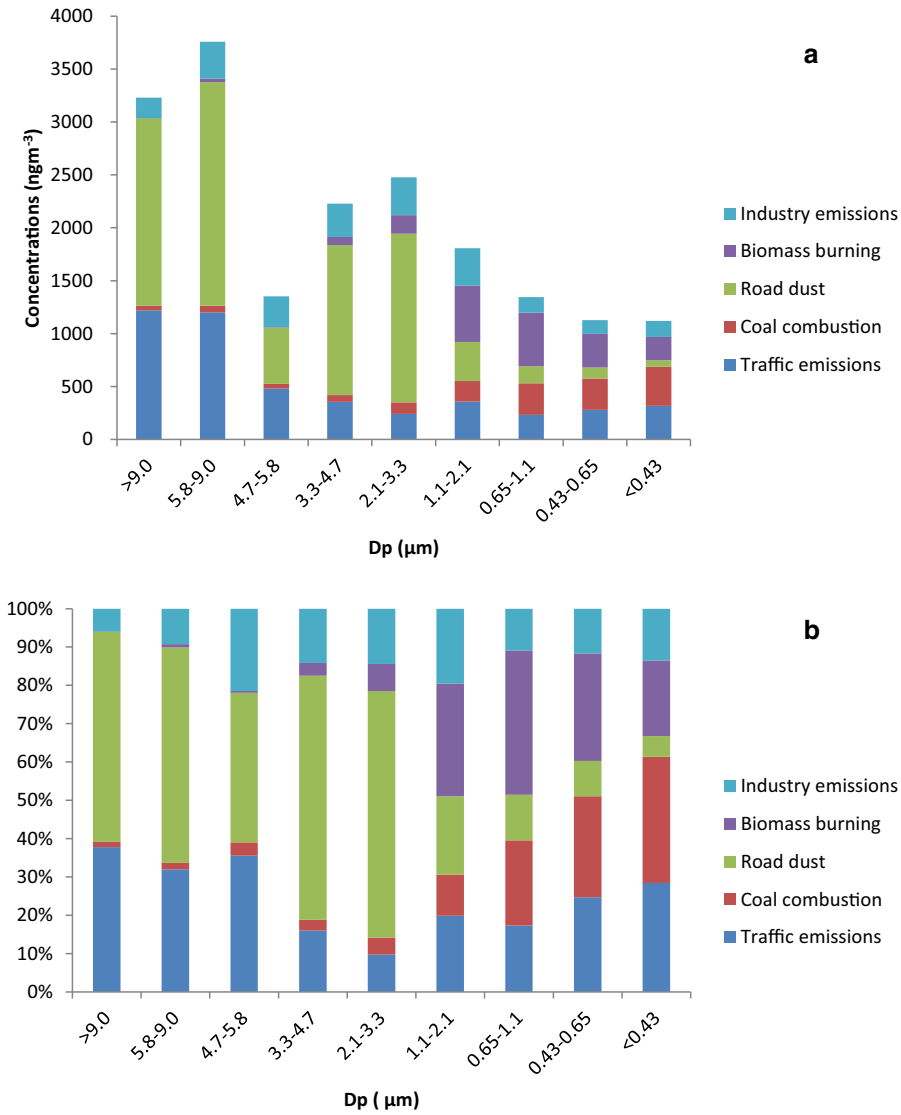

Fig. 4 Absolute **(a)** and relative concentration **(b)** of each source to the sum of elements in each size bin

(Al) in the haze period and 34.6% (Cu) – 44.8% (Al) in the non-haze period. This result is close to that of Betha et al. (2014), who reported the total deposition efficiency in the range of 40.0% (Mg)–56.0% (Ca) in the haze period and 33.0% (Mg)–51.0% (Ca) in the non-haze period. As for elements in coarse particles ($PM_{2.1–9.0}$), the sum value is 90.5% (Cd)–94.3% (As) on haze days and 91.6% (Pb)–94.7% (Cd) on non-haze days. The results are very close to the results of Zwozdziak et al.(2017). It was reported that 45.2% (As)–91.1% (Ca) on winter days and 43.9% (As)–88.9% (Ca) on summer days were found for the PM_{10} particles in the hotspot of an urban area. As shown in Fig. 12, H and T are the highest and lowest deposition region among the three regions in both fine and coarse particles.

Regarding trace elements on $PM_{2.1}$ that deposit in the respiratory system, noted for the haze and non-haze period, 12.3% (Cu)–15.5% (Al) and 12.5% (Ni)–14.4% (Mg) remain in the P region. It was observed that most elements show higher deposition fractions in haze period except Na, Mg, K, Ca, V, Cu, As, Cd and Pb; but no significant difference (one-factor ANVOA, $p > 0.05$) between haze and non-haze periods except Al, V and As. As for coarse particles ($PM_{2.1–9.0}$), the related deposited fractions are 6.76% (Ca)–13.1% (Cd) in the haze period and 6.09% (Na)–11.5% (Pb) in the non-haze period; higher deposition fractions in the

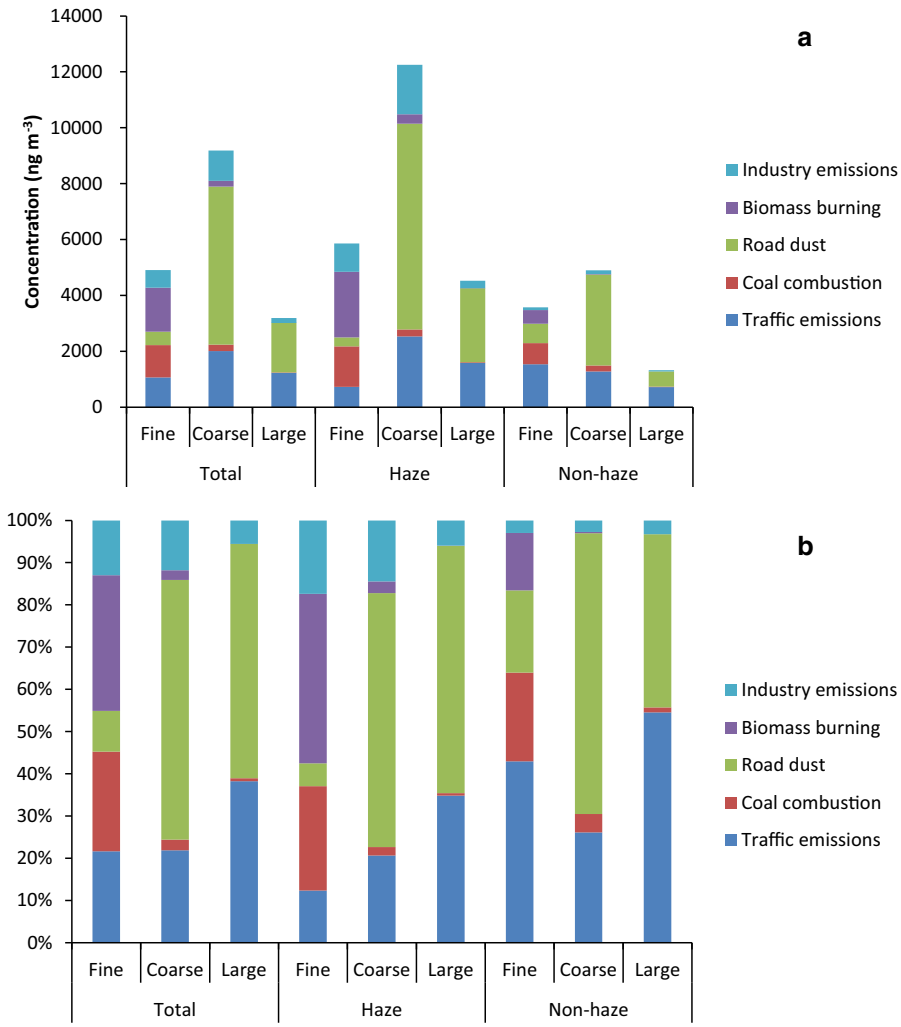

Fig. 5 Absolute **(a)** and relative concentration **(b)** of each source to the sum of elements in fine, coarse and large particles during the haze and non-haze days

haze period are also observed except for Mg, Al, Co, Ni, Cu and Pb. However, only the deposition fraction of Na, Mg, V, Mn and Cd shows a significant difference between the haze and non-haze period (one-factor ANVOA, $p < 0.05$). Therefore, the deposition fractions of elements at the P region were higher in the haze period for most elements. Similar conclusions were reported by previous studies. For example, both studies of Betha et al. (2014) and Behera et al. (2015a) reported that all elements except Al, Fe and Cu had higher deposition efficiencies in the haze days. Besides Ham et al.(2011), also found V, Zn and Se had greater deposition efficiencies in summer than winter events. Therefore, other factors should be considered besides the chemical composition of elements.

Health risk assessment (HRA)

HRA of trace elements from the inhalation of ambient fine and coarse particles has been employed for both periods to evaluate the impact of haze on adults living in Ningbo. For the haze and non-haze periods, it was assumed that all days are haze and non-haze in a year of 365 days, respectively. Also, it was hypothesized that the toxic Cr (VI) was only 1/7 of the total Cr concentration for the health risk assessment in this study as the total Cr not Cr (VI) was measured by ICP-MS (Taner et al. 2013).

Figure 7 shows the non-carcinogenic and carcinogenic risks for adults through the inhalation exposure pathway to fine and coarse particles in both non-haze

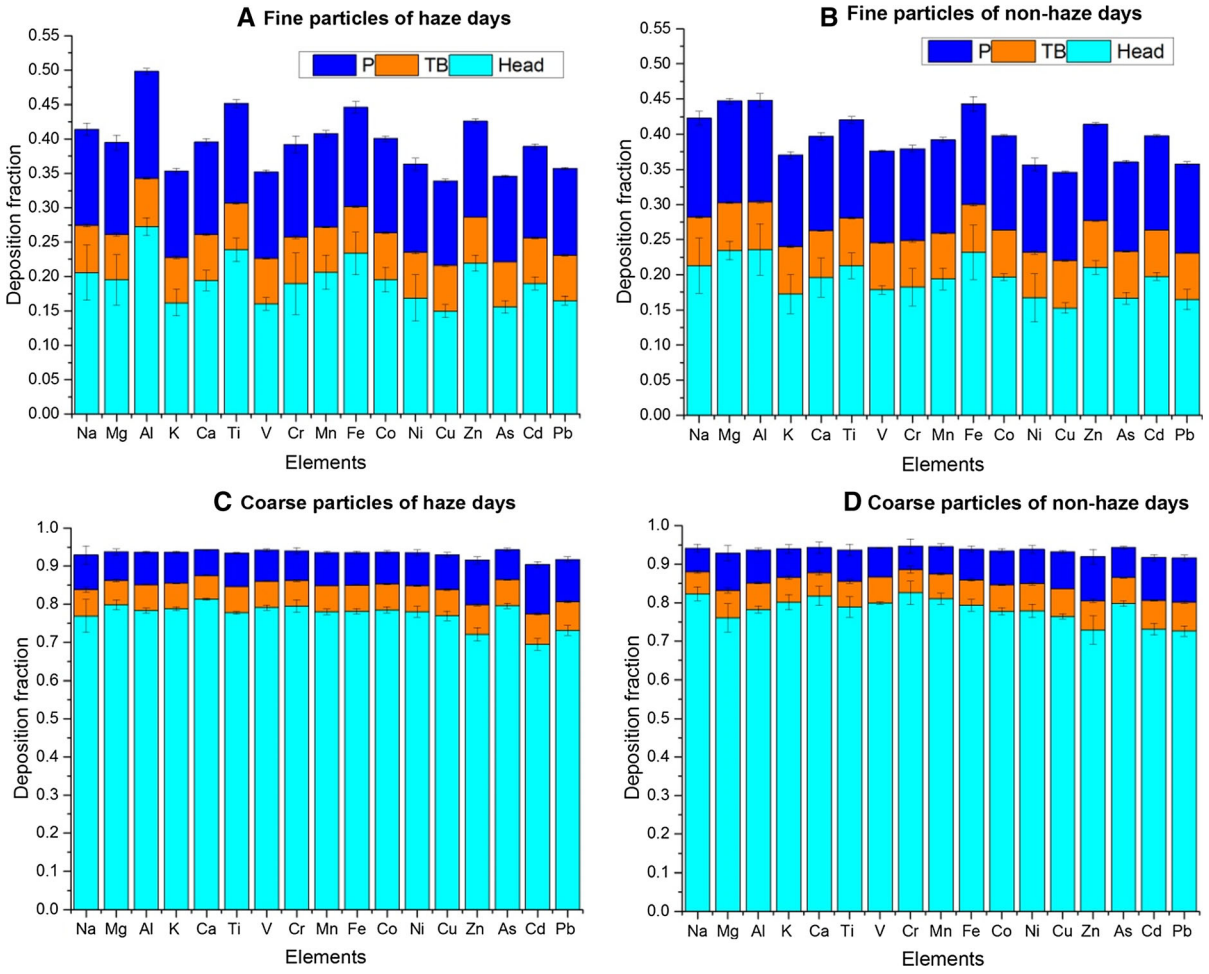

Fig. 6 Deposition fractions of elements in H, T and P for fine and coarse particles in haze and non-haze days

and haze periods. HI was 1.29–3.25 and ELCR was 4.67×10^{-5}–1.64×10^{-4} when deposition fractions of toxic elements were not considered. The results were in agreement with previous studies in Ningbo (Wang et al. 2018b; Wu et al. 2019). However, health risks were reduced to 7.87%–13.1% for HI and 6.68%–13.3% for ELCR when deposition fractions of elements were applied to the HRA assessment.

For the results of applying deposition fractions, Fig. 7 shows that the non-carcinogenic health risk was ranging from 0.100 for coarse particles in the non-haze period to 0.430 for fine particles in the haze period, which were not evident because the total HQ was lower than the acceptable limit (1.00). However, regarding the exposure to fine particles, the cancer risk exceeded the acceptable limit (1.00×10^{-6}) for both periods. The ELCR of the non-haze period was 8.50×10^{-6}, implying that nearly nine adults in a million are possible to suffer from cancer because of the inhalation of the fine particles in the non-haze period. However, the ELCR increased by 2.42-fold to 2.06×10^{-5} in the haze period, indicating the haze has a harmful impact on the health of residents. Cancer risks of the toxic metals are ranked as Cr (VI) > As > Co > Cd > Ni > Pb in the non-haze period and Cr(VI) > As > Cd > Co > Ni > Pb in the haze period. Besides, it should be noted that only the cancer risks of Cr (VI) and As were above the acceptable level (1.00×10^{-6}), indicating that the cancer risks of Co, Ni, Cd and Pb in fine particles are not significant in Ningbo. However, as shown in Fig. 13, the related ELCR values in coarse particles were 36.7% and 62.8% of that in the fine particles for the non-haze period and haze period, respectively, when the

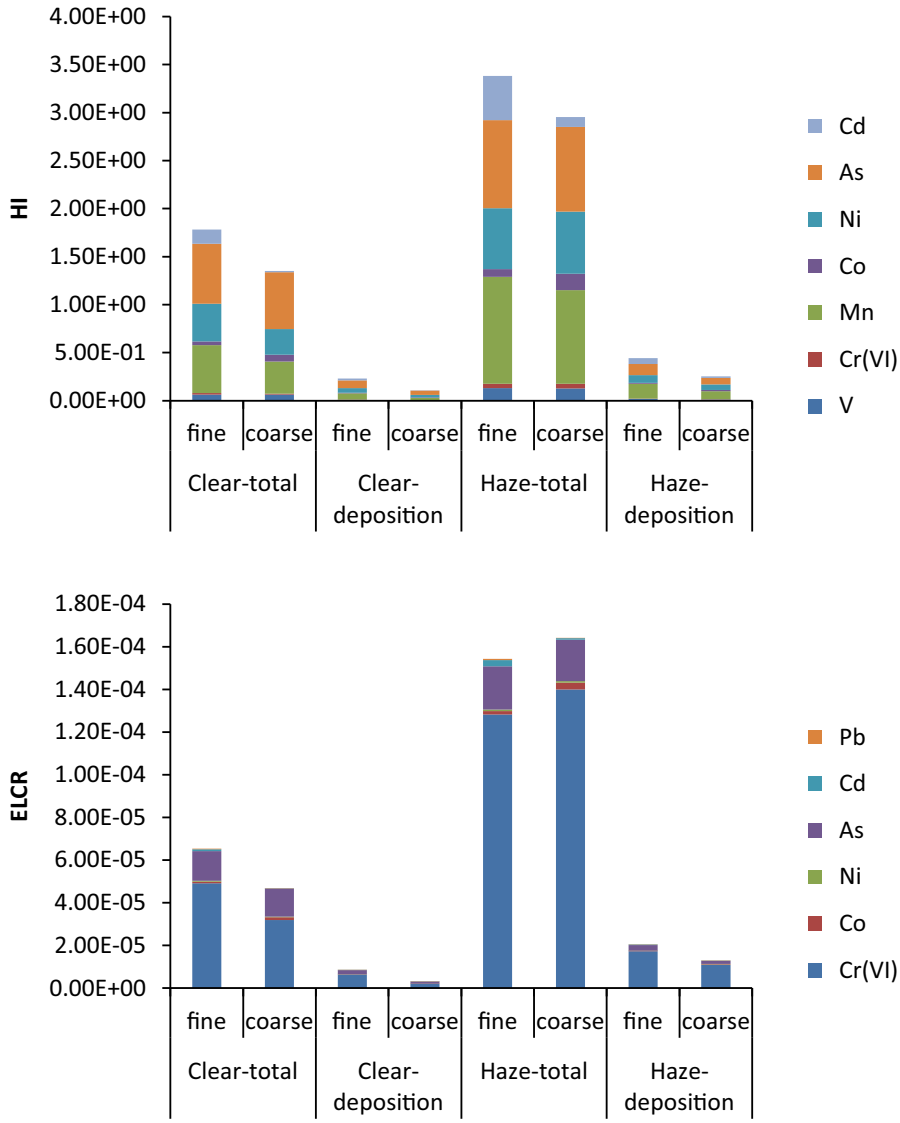

Fig. 7 Non-carcinogenic (HI) and carcinogenic (ELCR) health risks for adult via inhalation exposure to fine ($PM_{2.1}$) and coarse ($PM_{2.1–9.0}$) particles during the non-haze and haze days in Ningbo

elemental concentrations from $PM_{2.1–9.0}$ deposited in the pulmonary region were used for the health risk assessment. It should be noted that the cancer risks of Cr (VI) and As were still above the safety limit for coarse particles in both non-haze and haze periods. It might suggest that toxic elements from the coarse particles could also impose serious health risks and should not be ignored in such an assessment.

Comparatively, the ELCR value of Cr in the $PM_{2.1}$ in this study is of a 1 – 2 magnitude lower than those reported in other cities of the YRD region (Behera et al. 2015b; Niu et al. 2015). Behera et al. (2015b) reported ELCR of 15.8×10^{-6} in the non-haze period and 32.9×10^{-6} in the haze period for Cr in winter at Shanghai. It seems that the total concentration of Cr and total deposition of 0.46 was used for the ELCR calculation. Niu et al. (2015) also found the ELCR of Cr in $PM_{2.5}$ from Hangzhou was 201×10^{-6}. The exposure duration (ED) was assumed as 70 years when calculating the exposure concentration but actually, it was 24 years for adults. Moreover, they also used total concentration and total deposition of Cr in the calculation of ELCR.

To improve the validity and reliability of the health risk assessment, more factors need to be taken into account. Firstly, the bio-accessibility of the toxic elements in the lung fluid would provide a realistic condition (Kastury et al. 2017). Secondly, more toxic

components in inhalable particles, such as arsenic, mercury and organic compounds, could be considered for the quantitative estimation health risks. Finally, ingestion and dermal absorption of fine particles should also be included as main exposure routes for such evaluation.

Conclusion

Size-segregated particle samples were taken from Ningbo in both haze and non-haze periods. Total concentrations of seventeen trace elements were measured with ICP-MS. Conclusions are listed as following:

(1) Trace elements were much more concentrated in both fine and coarse particles as compared to large particles. The elemental concentrations in the haze period were significantly higher than the non-haze period. The concentrations of Cr (VI) and As in fine particles were above the national air quality standards in both haze and non-haze periods, while the levels of Mn, Ni, Cd and Pb were below the allowable thresholds during both periods.

(2) The estimated EFs confirmed that Na, Mg, Al, Ca, Ti, Fe and Co were mainly from crustal sources, and Cr, Cu, Zn, Cd and Pb were mainly from non-crustal sources, while K, Mn and Ni come from both sources. The size distribution of elements showed that crustal elements were enriched in the coarse particles, some non-crustal elements (i.e. Zn, Cd and Pb) were concentrated in the fine particles, while other elements (K, Cr, Mn, Ni and Cu) showed bimodal distributions.

(3) Five sources including traffic emissions, coal combustion, soil dust, biomass burning and industry emissions were identified for trace elements. Large and coarse particles are mainly formed with a large amount of soil dust, traffic emissions and moderate industry emissions. The sources of fine particles are characterized by large amounts of traffic emissions, coal combustion and biomass burning. Compare with the non-haze period, coal combustion, industry emissions and biomass burning during the haze period increased twofold–tenfold, which was in agreement with the results of cluster analysis of air mass backward trajectories.

(4) The results from MPPD show particles in the H region had the highest deposition fraction, followed by the P and T region. The deposition fraction of trace elements in the P region had no significant difference between the two periods for most elements. The health risk assessment for adults exposed to the toxic elements suggested that non-carcinogenic risk was below the safety limit, but the cancer risks were above the safety limit. Moreover, the related ELCR values in coarse particles were 36.71% and 62.76% of those in the fine particles for the non-haze period and haze period, respectively. This suggests that toxic elements from the coarse particles should not be ignored in the health risk assessment.

Acknowledgements The research was conducted at the International Doctoral Innovation Centre (IDIC), University of Nottingham Ningbo China. The authors of the present study acknowledge the financial support from IDIC, Ningbo Education Bureau, Ningbo Science and Technology Bureau, and the University of Nottingham. This research was also partially supported by the Ningbo Municipal Innovation Team Project (2017C510001) and UK Engineering and Physical Sciences Research Council (EP/G037345/1 and EP/L016362/1).

References

Andreae, M. O., Andreae, T. W., Annegarn, H., Beer, J., Cachier, H., Le Canut, P., et al. (1998). Airborne studies of aerosol emissions from savanna fires in southern Africa: 2. Aerosol chemical composition. *Journal of Geophysical Research-Atmospheres, 103,* 32119–32128.

Behera, S. N., Betha, R., Huang, X., & Balasubramanian, R. (2015). Characterization and estimation of human airway deposition of size-resolved particulate-bound trace elements during a recent haze episode in Southeast Asia. *Environmental Science and Pollution Research., 22,* 4265–4280.

Behera, S. N., Cheng, J., Huang, X., Zhu, Q., Liu, P., & Balasubramanian, R. (2015). Chemical composition and acidity of size-fractionated inorganic aerosols of 2013–14 winter haze in Shanghai and associated health risk of toxic elements. *Atmospheric Environment., 122,* 259–271.

Betha, R., Behera, S. N., & Balasubramanian, R. (2014). Southeast Asian Smoke Haze: Fractionation of Particulate-Bound Elements and Associated Health Risk. *Environmental Science & Technology., 48,* 4327–4335.

Cao, J.-J., Shen, Z.-X., Chow, J. C., Watson, J. G., Lee, S.-C., Tie, X.-X., et al. (2012). Winter and Summer $PM_{2.5}$ Chemical Compositions in Fourteen Chinese Cities.

Journal of the Air & Waste Management Association., 62, 1214–1226.

Cheng, H.-G., Zhou, T., Li, Q., Lu, L., & Lin, C.-Y. (2014). Anthropogenic Chromium Emissions in China from 1990 to 2009. *PLoS ONE, 9,* e87753.

Fang, G.-C., Huang, Y.-L., & Huang, J.-H. (2010). Study of atmospheric metallic elements pollution in Asia during 2000–2007. *Journal of Hazardous Materials., 180,* 115–121.

Fu, Q., Zhuang, G., Wang, J., Xu, C., Huang, K., Li, J., et al. (2008). Mechanism of formation of the heaviest pollution episode ever recorded in the Yangtze River Delta China. *Atmospheric Environment, 42,* 2023–2036.

Gao, Y., Lee, S.-C., Huang, Y., Chow, J. C., & Watson, J. G. (2016). Chemical characterization and source apportionment of size-resolved particles in Hong Kong sub-urban area. *Atmospheric Research, 170,* 112–122.

Greene, N. A., & Morris, V. R. (2006). Assessment of public health risks associated with atmospheric exposure to $PM_{2.5}$ in Washington, DC, USA. *International Journal of Environmental Research and Public Health, 3,* 86–97.

Ham, W. A., Ruehl, C. R., & Kleeman, M. J. (2011). Seasonal Variation of Airborne Particle Deposition Efficiency in the Human Respiratory System. *Aerosol Science and Technology, 45,* 795–804.

Ho, K. F., Lee, S. C., Cao, J. J., Chow, J. C., Watson, J. G., & Chan, C. K. (2006). Seasonal variations and mass closure analysis of particulate matter in Hong Kong. *Science of The Total Environment, 355,* 276–287.

Hofmann, W. (2011). Modelling inhaled particle deposition in the human lung-A review. *Journal of Aerosol Science, 42,* 693–724.

Hu, M., Peng, J. F., Sun, K., Yue, D. L., Guo, S., Wiedensohler, A., & Wu, Z. J. (2012). Estimation of Size-Resolved Ambient Particle Density Based on the Measurement of Aerosol Number, Mass, and Chemical Size Distributions in the Winter in Beijing. *Environmental Science & Technology, 46,* 9941–9947.

Huang, R. J., Zhang, Y., Bozzetti, C., Ho, K.-F., Cao, J. J., Han, Y., et al. (2014). High secondary aerosol contribution to particulate pollution during haze events in China. *Nature, 514,* 218–222.

Huang, R. J., Cheng, R., Jing, M., Yang, L., Li, Y.-J., Chen, Q., et al. (2018). Source-Specific Health Risk Analysis on Particulate Trace Elements: Coal Combustion and Traffic Emission As Major Contributors in Wintertime Beijing. *Environmental Science & Technology, 52,* 10967–10974.

Huang, S., Tu, J., Liu, H., Hua, M., Liao, Q., Feng, J., et al. (2009). Multivariate analysis of trace element concentrations in atmospheric deposition in the Yangtze River Delta East China. *Atmospheric Environment, 43,* 5781–5790.

Jeong, C. H., Wang, J. M., Hilker, N., Debosz, J., Sofowote, U., Su, Y. S., et al. (2019). Temporal and spatial variability of traffic-related $PM_{2.5}$ sources: Comparison of exhaust and non-exhaust emissions. *Atmospheric Environment, 198,* 55–69.

Kampa, M., & Castanas, E. (2008). Human health effects of air pollution. *Environmental Pollution, 151,* 362–367.

Kastury, F., Smith, E., & Juhasz, A. L. (2017). A critical review of approaches and limitations of inhalation bioavailability and bioaccessibility of metal(loid)s from ambient particulate matter or dust. *Science of the Total Environment, 574,* 1054–1074.

Khare, P., & Baruah, B. P. (2010). Elemental characterization and source identification of PM2.5 using multivariate analysis at the suburban site of North-East India. *Atmospheric Research, 98,* 148–162.

Khillare, P. S., & Sarkar, S. (2012). Airborne inhalable metals in residential areas of Delhi, India: distribution, source apportionment and health risks. *Atmospheric Pollution Research, 3,* 46–54.

Li, H. M., Wang, J., Wang, Q. G., Qian, X., Qian, Y., Yang, M., et al. (2015). Chemical fractionation of arsenic and heavy metals in fine particle matter and its implications for risk assessment: A case study in Nanjing China. *Atmospheric Environment, 103,* 339–346.

Li, X. R., Wang, L. L., Wang, Y. S., Wen, T. X., Yang, Y. J., Zhao, Y.-N., & Wang, Y. F. (2012). Chemical composition and size distribution of airborne particulate matters in Beijing during the 2008 Olympics. *Atmospheric Environment, 50,* 278–286.

Li, X. Y., Yan, C. Q., Patterson, R. F., Zhu, Y. J., Yao, X. H., Zhu, Y. F., et al. (2016). Modeled deposition of fine particles in human airway in Beijing China. *Atmospheric Environment, 124,* 387–395.

Liu, Y. Y., Xing, J., Wang, S. X., Fu, X., & Zheng, H. T. (2018). Source-specific speciation profiles of $PM_{2.5}$ for heavy metals and their anthropogenic emissions in China. *Environmental Pollution, 239,* 544–553.

Lyu, Y., Zhang, K., Chai, F.-H., Cheng, T.-T., Yang, Q., Zheng, Z. L., & Li, X. (2017). Atmospheric size-resolved trace elements in a city affected by nonferrous metal smelting: Indications of respiratory deposition and health risk. *Environmental Pollution, 224,* 559–571.

Ministry of Envrionmental Protection (MEP). (2012). *Ambient Air Quality Standards (GB3095-2012)* (pp. 1–12). Beijing: China Environmental Science Press.

Mishra, D., Goyal, P., & Upadhyay, A. (2015). Artificial intelligence based approach to forecast $PM_{2.5}$ during haze episodes: A case study of Delhi India. *Atmospheric Environment, 102,* 239–248.

Mukhtar, A., & Limbeck, A. (2013). Recent developments in assessment of bio-accessible trace metal fractions in airborne particulate matter: A review. *Analytica Chimica Acta, 774,* 11–25.

Niu, L., Ye, H., Xu, C., Yao, Y., & Liu, W. (2015). Highly time- and size-resolved fingerprint analysis and risk assessment of airborne elements in a megacity in the Yangtze River Delta, China. *Chemosphere, 119,* 112–121.

O'Shaughnessy, P. T., & Raabe, O. G. (2003). A comparison of cascade impactor data reduction methods. *Aerosol Science and Technology, 37,* 187–200.

Pan, Y., Wang, Y., Sun, Y., Tian, S., & Cheng, M. (2013). Size-resolved aerosol trace elements at a rural mountainous site in Northern China: Importance of regional transport. *Science of the Total Environment, 461,* 761–771.

Saffari, A., Daher, N., Shafer, M. M., Schauer, J. J., & Sioutas, C. (2014). Global Perspective on the Oxidative Potential of Airborne Particulate Matter: A Synthesis of Research Findings. *Environmental Science & Technology, 48,* 7576–7583.

Stein, A. F., Draxler, R. R., Rolph, G. D., Stunder, B. J. B., Cohen, M. D., & Ngan, F. (2015). NOAA's HYSPLIT

Atmospheric Transport and Dispersion Modeling System. *Bulletin of the American Meteorological Society, 96,* 2059–2077.

Sun, Y. L., Zhuang, G. S., Tang, A. H., Wang, Y., & An, Z. S. (2006). Chemical characteristics of $PM_{2.5}$ and PM_{10} in haze-fog episodes in Beijing. *Environmental Science & Technology, 40,* 3148–3155.

Tan, J. H., Duan, J. C., Ma, Y. L., Yang, F. M., Cheng, Y., He, K. B., et al. (2014). Source of atmospheric heavy metals in winter in Foshan, China. *Science of the Total Environment, 493,* 262–270.

Tan, J. H., Duan, J. C., Zhen, N. J., He, K. B., & Hao, J. M. (2016). Chemical characteristics and source of size-fractionated atmospheric particle in haze episode in Beijing. *Atmospheric Research, 167,* 24–33.

Taner, S., Pekey, B., & Pekey, H. (2013). Fine particulate matter in the indoor air of barbeque restaurants: Elemental compositions, sources and health risks. *Science of the Total Environment, 454,* 79–87.

Tao, M., Chen, L., Xiong, X., Zhang, M., Ma, P., Tao, J., & Wang, Z. (2014). Formation process of the widespread extreme haze pollution over northern China in January 2013: Implications for regional air quality and climate. *Atmospheric Environment, 98,* 417–425.

Taylor, S. R., & McLennan, S. M. (1995). The geochemical evolution of the continental-crust. *Reviews of Geophysics, 33,* 241–265.

Tian, H. Z., Liu, K. Y., Zhou, J. R., Lu, L., Hao, J. M., Qiu, P. P., et al. (2014). Atmospheric Emission Inventory of Hazardous Trace Elements from China's Coal-Fired Power Plants-Temporal Trends and Spatial Variation Characteristics. *Environmental Science & Technology, 48,* 3575–3582.

United States Environment Protection Agency (USEPA). (2009). Risk Assessment Guidance for Superfund (RAGS), Volume I: Human Health Evaluation Manual (Part F, Supplemental Guidance for Inhalation Risk Assessment). Available on-line at: ttp://www.epa.gov/oswer/riskassessment/ragsf/index.htm.

United States Environment Protection Agency (USEPA). (2015).User's Guide/technical Background Document for US EPA Region 9's RSL (Regional Screening Levels) Tables. Available on-line at: https://www.epa.gov/region9/superfund/prg/.

Wang, H. L., An, J. L., Shen, L. J., Zhu, B., Pan, C., Liu, Z. R., et al. (2014). Mechanism for the formation and microphysical characteristics of submicron aerosol during heavy haze pollution episode in the Yangtze River Delta China. *Science of the Total Environment, 490,* 501–508.

Wang, J., Pan, Y., Tian, S., Chen, X., Wang, L., & Wang, Y. (2016). Size distributions and health risks of particulate trace elements in rural areas in northeastern China. *Atmospheric Research, 168,* 191–204.

Wang, S.-B., Yan, Q.-S., Zhang, R.-Q., Jiang, N., Yin, S.-S., & Ye, H.-Q. (2019). Size-fractionated particulate elements in an inland city of China: Deposition flux in human respiratory, health risks, source apportionment, and dry deposition. *Environmental Pollution, 247,* 515–523.

Wang, W., Yu, J., Cui, Y., He, J., Xue, P., Cao, W., et al. (2018). Characteristics of fine particulate matter and its sources in an industrialized coastal city Ningbo, Yangtze River Delta, China. *Atmospheric Research, 203,* 105–117.

Wang, X., He, S., Chen, S., Zhang, Y., Wang, A., Luo, J., et al. (2018). Spatiotemporal Characteristics and Health Risk Assessment of Heavy Metals in $PM_{2.5}$ in Zhejiang Province. *International Journal of Environmental Research and Public Health, 15,* 583–600.

Wang, Y. Q., Zhang, X. Y., & Draxler, R. R. (2009). TrajStat: GIS-based software that uses various trajectory statistical analysis methods to identify potential sources from long-term air pollution measurement data. *Environmental Modelling & Software, 24,* 938–939.

World Health Organization (WHO). (2000). *Air quality guidelines for Europe, second edition* (WHO regional publications. European series ; No. 91), 288.

Wu, Y., Lu, B. B., Zhu, X. L., Wang, A. H., Yang, M., Gu, S. H., et al. (2019). Seasonal Variations, Source Apportionment, and Health Risk Assessment of Heavy Metals in $PM_{2.5}$ in Ningbo, China. *Aerosol and Air Quality Research, 19,* 2083–2092.

Xu, J. S., Xu, H. H., Xiao, H., Tong, L., Snape, C. E., Wang, C. J., & He, J. (2016). Aerosol composition and sources during high and low pollution periods in Ningbo, China. *Atmospheric Research, 178–179,* 559–569.

Xu, J. S., Tai, X., Betha, R., He, J., & Balasubramanian, R. (2015). Comparison of physical and chemical properties of ambient aerosols during the 2009 haze and non-haze periods in Southeast Asia. *Environmental Geochemistry and Health, 37,* 831–841.

Yan, P., Zhang, R., Huan, N., Zhou, X., Zhang, Y., Zhou, H., & Zhang, L. (2012). Characteristics of aerosols and mass closure study at two WMO GAW regional background stations in eastern China. *Atmospheric Environment, 60,* 121–131.

Yang, Y., Wang, Y., Huang, W., Hu, B., Wen, T., & Zhao, Y. N. (2010). Size Distributions and Elemental Compositions of Particulate Matter on Clear Hazy and Foggy days in Beijing, China. *Advances in Atmospheric Sciences, 27,* 663–675.

Youn, J. S., Csavina, J., Rine, K. P., Shingler, T., Taylor, M. P., Sáez, A. E., et al. (2016). Hygroscopic Properties and Respiratory System Deposition Behavior of Particulate Matter Emitted By Mining and Smelting Operations. *Environmental Science & Technology, 50,* 11706–11713.

Zhang, J., Zhou, X., Wang, Z., Yang, L., Wang, J., & Wang, W. (2018). Trace elements in $PM_{2.5}$ in Shandong Province: Source identification and health risk assessment. *The Science of the Total Environment, 621,* 558–577.

Zoller, W. H., Gladney, E. S., & Duce, R. A. (1974). Atmospheric concentrations and sources of trace-metals at south pole. *Science, 183,* 198–200.

Zwozdziak, A., Gini, M. I., Samek, L., Rogula-Kozlowska, W., Sowka, I., & Eleftheriadis, K. (2017). Implications of the aerosol size distribution modal structure of trace and major elements on human exposure, inhaled dose and relevance to the PM2.5 and PM10 metrics in a European pollution hotspot urban area. *Journal of Aerosol Science, 103,* 38–52.